



## Cold gas dynamic spraying of WC–Ni cemented carbide coatings



D. Lioma<sup>a,b,\*</sup>, N. Sacks<sup>a,b</sup>, I. Botef<sup>b,c</sup>

<sup>a</sup> School of Chemical and Metallurgical Engineering, University of the Witwatersrand, Private Bag 3, Wits, 2050 Johannesburg, South Africa

<sup>b</sup> DST–NRF Centre of Excellence in Strong Materials, South Africa

<sup>c</sup> School of Mechanical, Industrial and Aeronautical Engineering, University of the Witwatersrand, South Africa

### ARTICLE INFO

#### Article history:

Received 30 April 2014

Received in revised form 20 August 2014

Accepted 22 August 2014

Available online 16 September 2014

#### Keywords:

Cemented carbides

Cold spray

Coatings

Ni

WC

Taguchi method

### ABSTRACT

The feasibility of using a low pressure cold spray system for the deposition of WC–Ni coatings was studied. The Ni content was varied from 4 to 50 wt.% and the resultant coating properties were compared to WC–12Co–xNi powders, deposited using the same Ni contents. A Taguchi mixed level design of experiments method was used to optimize the spray parameters of each of the eight powder combinations. The optimal coatings predicted using this method were the WC–25Ni and WC–12Co–50Ni combinations. However the maximum experimental coating hardness was obtained for the 4 wt.% Ni coatings. A limitation of the Taguchi method is that it does not account for the effect of strain hardening that occurs as a result of the impact of the hard carbide particles. Low porosity coating build-up with non-homogenous distribution of the carbide phase was observed for all coatings. XRD analysis of the coatings indicated that no phase transformations or grain refinement took place during deposition. The morphology of the starting powders influenced coating properties. The dense WC particles had limited deformability and resulted in the fracture of the hard WC particles during deposition. The porous structure of the spherical and agglomerated WC–12Co powders was more deformable allowing for particle densification and elongation during deposition which resulted in higher WC retention within the Ni matrix.

© 2014 Elsevier Ltd. All rights reserved.

### 1. Introduction

WC-based coatings are conventionally deposited using high temperature thermal processes such as high velocity oxy-fuel (HVOF), plasma transferred arc welding (PTAW) and spray fusion (SF) which involve the melting of the binder phase to achieve superior adhesion. The heat required to melt the binder phase often results in the deterioration of the carbide and binder phases by decarburization, phase changes, high temperature oxidation and grain growth [1–7]. Brittle and hard W<sub>2</sub>C, W and undesirable  $\eta$  phases are usually the result of this deterioration, which decreases the overall mechanical and wear properties of the coatings [8–10]. In order to minimize these coating degradation effects, researchers have been investigating the deposition of WC-based coatings using cold gas dynamic spraying (CGDS) as an alternative to high temperature deposition processes [11–13]. CGDS is a deposition method in which fine, solid powder particulates (1–50  $\mu\text{m}$  in diameter) are accelerated to supersonic speeds (300–1200  $\text{m}\cdot\text{s}^{-1}$ ) by means of a carrier gas and are impacted onto a surface to form dense coatings [14]. The process is solely reliant on the severe plastic deformation of the particles to achieve sufficient substrate adhesion and coating build-up. Adhesion is said to occur as a result of the high pressures experienced during impact, causing material interlocking and mechanical bonding of the

corresponding atoms [15,16]. This process involves limited to no melting during coating deposition; thus avoiding the decomposition of the carbide phase. The chemical composition and bulk properties of the coatings typically remain identical to the parent powders [1–7].

Two types of cold spraying systems, high and low pressure, currently exist. High pressure systems can attain pressures ranging up to 1000 psi, accelerating the gas flow to supersonic velocities (1000  $\text{m}\cdot\text{s}^{-1}$ ). Low pressure systems can attain a pressure range of 80–140 psi. In these low pressure systems, the propellant gas with the suspended powder particles can reach velocities of about 600  $\text{m}\cdot\text{s}^{-1}$ . The low pressure systems are deemed safer, more portable, and easier and cheaper to automate, making this an attractive deposition method [17,18]. Deposition of WC–Co coatings has been achieved using high pressure systems with dense coatings having thickness and hardness values comparable to HVOF coatings [11]. No evidence of decarburization or phase changes was observed, although Ang et al. [19] found the occurrence of grain refinement.

It is generally more challenging to achieve the adhesion of WC–Co coatings using low pressure systems [20]. Since the severe plastic deformation of the particles is required for particle adhesion, the deposition of the carbide particles is limited, as they are hard and brittle in nature and therefore shatter and erode the substrate upon impact [1]. This is because the generated temperatures and pressures are insufficient for the deformation of the hard WC particles upon impact. To overcome this challenge, the carbide phase is co-deposited with a more ductile metal, such as Co, Cu and Al, in the form of a cemented carbide or a metal matrix composite [21,22]. The purpose of the softer binder

\* Corresponding author at: School of Chemical and Metallurgical Engineering, University of the Witwatersrand, Private Bag 3, Wits, 2050 Johannesburg, South Africa.

E-mail address: [Dineo.Lioma@students.wits.ac.za](mailto:Dineo.Lioma@students.wits.ac.za) (D. Lioma).

material is to facilitate the adhesion of the hard WC particles which are embedded in the softer metal matrix during deposition. The cermet particles were either mechanically mixed [22] with the softer binder phase or were encapsulated [21] with the binder metal to facilitate the adhesion of the hard and brittle phases.

Some of the factors that influence the deposition efficiency of carbide coatings include spray parameters, such as gas temperature and pressure, standoff distance (SOD), substrate properties, powder particle size and morphology, and binder content [13,21,22]. Process variables also determine the critical particle velocity required for adhesion. When the particle impact velocity,  $V_p$ , is too low for a given coating–substrate combination, the feedstock particles act as erodents and are reflected from the surface with no deposition taking place. When  $V_p$  is greater or equal to the critical velocity the particles deform plastically and adhere to the substrate forming a coating [23]. Previous research has found that if the  $V_p$  is too high, hard brittle materials, such as the WC particles under study, pulverize upon impact and fail to adhere on the substrate due to their lack of deformability [21]. This also proves that there is a window of deposition of particles during CGDS [23].

Goyal et al. [24–26] investigated the optimization of multiple response parameters in low-pressure cold sprayed Cu coatings using the Taguchi method and utility concept. In the study, the input variables were powder feed type, substrate material, stand-off distance, stagnation pressure and temperature and the responses to be optimized were coating density, thickness and surface roughness. The optimal parameter values were determined by calculating the signal to noise ratios (SNRs) for each response, which also served as an indication of the contribution that each parameter had on the responses measured. The variables yielding the greatest SNR values were an indication of the optimal parameters. Using this technique they were able to successfully optimize the response variables, identify the percentage contribution of each input parameter, and predict the values of the optimal responses [24–26].

To the current authors' knowledge, this type of systematic approach to determine the optimal spray parameters for WC–Ni systems, using low pressure CGDS, has not been conducted, and was therefore the main focus of the current research study. Here, the feasibility of using a Centerline SST low pressure CGDS system, with air as the carrier gas, to deposit WC– $x$  wt.% Ni coatings onto mild steel substrates was assessed; the Ni content was varied from 4 to 50 wt.%. The spray parameter combinations were determined using the Taguchi mixed level design of experiments technique, to establish the optimum spray conditions for each powder composition. The coating properties were characterized and the results compared to WC–12 wt.% Co– $x$  wt.% Ni coatings, also sprayed for this study.

## 2. Experimental procedure

### 2.1. Powder and substrate

In this study three different powders were used, namely, an agglomerated and sintered WC–12 wt.% Co powder (Sulzer Metco), an oxide

reduced WC powder (Flomaster), and a Ni powder (Centerline SST-N5001). All three powders had a particle size distribution of  $-45 + 5 \mu\text{m}$ . The morphologies of the three powders are illustrated in Fig. 1. The powders were mechanically mixed using a rotary mill according to the compositions listed in Table 1. Mild steel substrates,  $20 \times 20 \text{ mm}^2$  in size, were grit blasted with  $-300 + 100 \mu\text{m}$  alumina grit (Centerline SST-G0002) prior to the deposition process to facilitate adhesion of the coatings.

### 2.2. Cold spray deposition process

A low pressure cold spray machine (Centreline SST Series P) was used to deposit the cemented carbides onto the mild steel substrates using air as the carrier gas. A CompAir external air compressor with a maximum capacity of 10 bars (150 psi) was used to generate the air flow required to achieve the air pressures used in this study. Eight passes were sprayed onto the substrates using an automated gun moving at a transverse velocity of  $3 \text{ m} \cdot \text{s}^{-1}$ . A convergent–divergent De Laval nozzle with a length of 120 mm, an entrance and exit diameter of 2.5 mm and 6 mm respectively was used to transmit the powders to the substrate. An integrated, dual-hopper, non-pressurized vibratory powder feeder with a feed rate setting of 5% was used to introduce the powder particles to the moving gas stream. Temperature, stagnation pressure and standoff distance were the operating parameters that were varied at different levels for the study, as presented in Table 2. The combination of spray parameters presented in Table 2 was determined using the Taguchi mixed level design of experiments [24–26] with the aim of finding the optimal spray parameters for each powder blend combination. In this multi-response process optimization method, four input parameters, namely wt.% Ni, temperature, stagnation pressure and stand-off distance, were varied within selected ranges based on the parameters recommended by the cold spray machine manufacturer for the deposition of Ni powder and the system's maximum operational capacity. Minitab® 16.2.4 software was applied to generate an L16 orthogonal array matrix which used coating thickness and hardness as the response variables. Each set of parameters was repeated three times and their responses averaged. Since coating thickness and hardness are both 'the higher, the better' type responses, the spray parameters giving the greatest signal to noise ratio (SNR) were selected as optimal and these values are reflected in Table 2 for each powder blend.

### 2.3. Coating characterization

The cross sections of the coatings were hot mounted with Struers Polyfast conductive resin, ground using Struers 220 and 1200 grit sizes, and then polished to a  $1 \mu\text{m}$  finish with Struers diamond suspension. Vickers micro-hardness tests, using a 300 gf load with a dwell time of 10 s, were conducted on the transverse sections of the coatings. A total of 12 indents were made per coating type, according to ASTM C1327 [27] which requires that each indent be spaced at a distance of

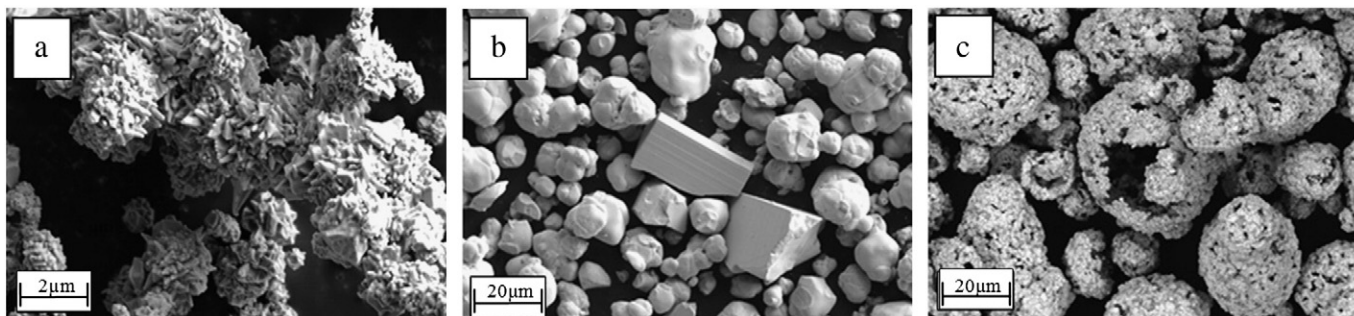


Fig. 1. Morphology of (a) Ni powder, (b) oxide reduced WC powder and (c) agglomerated and sintered WC–12 wt.% Co powders.

**Table 1**  
Composition of the mechanical powder blends.

Mechanical blend	wt.% WC	wt.% Ni	wt.% Co
WC-4Ni	96	4	0
WC-10Ni	90	10	0
WC-25Ni	75	25	0
WC-50Ni	50	50	0
WC-12Co-4Ni	84	4	12
WC-12Co-10Ni	78	10	12
WC-12Co-25Ni	63	25	12
WC-12Co-50Ni	38	50	12

at least four times the diagonal of the previous indent. This was done to avoid the effects of WC particle cracking and strain hardening. Micro-hardness profile tests were conducted for each coating composition along the cross-sections, from the coating surface to the coating–substrate interface. Each indent was spaced 0.2 mm apart. These profiles were performed to investigate the effect of repeated powder impact during deposition.

Low magnification ( $\times 50$ ,  $\times 100$ ,  $\times 200$ ,  $\times 500$  and  $\times 1000$ ) optical microscopy (LEICA DM6000 M, attached with a LEICA DFC490 camera) was applied to observe the coating build-up. The optical images and coating thickness measurements were acquired using Leica Application Suite image processing software. X-ray diffraction (Bruker D2, Phaser with a Lynx Eye detector) analysis of the powders and coatings was conducted to identify the phases and to detect if WC decarburization had occurred during deposition. A cobalt anode, with X-ray generator settings of 30 kV and 10 mA, was used for the analysis. The measurements were made from  $10^\circ$  to  $90^\circ$  at a rate of  $0.026^\circ$  per second. A Carl Zeiss Sigma, field emission scanning electron microscope (FESEM) coupled with an energy dispersive X-ray spectroscope (EDS), was used to characterize the microstructure of the coatings and the powder morphology, and to determine the percentage of the WC retained during the deposition process. The wt.% values of the W atoms, together with the known C:W weight ratio of 0.0613 was used to calculate the percentage of WC retained within the coating. The FESEM was also used to compose elemental composition maps of the coatings to assess the homogeneity.

The percentage porosity of each coating was determined using ImageJ analysis software in which the area fraction of the pores was calculated. Low magnification ( $\times 1000$ ) SEM micrographs were chosen to obtain representative images of the coatings, while ensuring that the resolution of the pores could be well defined for the image analysis technique. The binder mean free path for each coating was determined using Eq. (1) [28]. The linear intercept method was used to estimate the binder mean free path in which SEM micrographs ( $\times 5000$ ) were used for the estimation.

$$\lambda = (1-f)/NL \quad (1)$$

[28].

In Eq. (1),  $f$  is the volume fraction of dispersed phase determined from the cross section image and  $NL$  is the number of non-contiguous carbide grains intersected on a metallographic plane by a line of unit length.

**Table 2**  
Cold spray parameters determined using the Taguchi method for each blend.

Mechanical blend	Pressure (psi)	Temperature ( $^\circ\text{C}$ )	Standoff distance (mm)
WC-4Ni	145	550	15
WC-10Ni	115	450	15
WC-25Ni	115	550	15
WC-50Ni	130	450	10
WC-12Co-4Ni	145	550	15
WC-12Co-10Ni	115	450	15
WC-12Co-25Ni	145	450	15
WC-12Co-50Ni	145	550	15

### 3. Results

#### 3.1. Taguchi process optimization parameters

Fig. 2 compares the average, between the coating thickness and hardness SNR values, obtained for each process parameter. The contribution of each parameter on the response variables provides insight into the effects of the spray conditions on the different powders. Since coating thickness and hardness are both ‘the higher the better’ type responses, the maximum SNR values are an indication of the optimal parameters which should be used for each powder blend; a summary of which is provided in Table 2.

The graphs presented in Fig. 2(a)–(d) reflect the SNR for each of the selected parameters, the optimal value being an indication of the best parameter setting. From Fig. 2(a) it can be deduced that the addition of 25 wt.% and 50 wt.% Ni for WC and WC-12Co powders respectively would yield the optimal coatings. Fig. 2(b)–(d) reflects the SNR data for these two optimum coatings; similar graphs were generated for all the composition blends. The increase in stagnation pressure was preferred for the WC-12Co-50Ni powder, with the optimal parameter setting being at system’s maximum capacity of 145 psi [Fig. 2(b)]. The optimal stagnation pressure for the deposition of the WC-25Ni powder was obtained at 115 psi, further increases would result in poorer coating properties. The deposition temperatures played a significant role in the coating hardness and thickness of the WC-12Co-50Ni powder; however had no effect on the deposition of the WC-25Ni powder [Fig. 2(c)]. Higher spray distance are preferred for both powders [Fig. 2(d)].

None of the coating thickness and hardness values obtained experimentally fell within the range predicted using the Taguchi method. For the WC-25Ni powder, both the experimental thickness and hardness values were greater than those predicted by the method, while lower experimental hardness and thickness values were observed for the WC-12Co-50Ni coatings. The comparative values are listed in Table 3.

#### 3.2. Coating properties

SEM images of the cross-sectional microstructures of all eight compositions are presented in Fig. 3 with the corresponding XRD patterns in Fig. 4 for the WC-xNi compositions, and Fig. 5 for the WC-12Co-xNi compositions. As presented in Fig. 3, good coating build-up with some porosity (black phase) was achieved across all eight compositions. A non-homogenous distribution of the WC and WC-12Co particles (white phase) was observed within the Ni matrix (gray phase) for all coatings. The WC-4Ni [Fig. 3(a)] and WC-12Co-4Ni [Fig. 3(e)] combinations were able to retain the highest amount of carbide particles; as the Ni content in the starting powders increased, the carbide particles retained within the Ni matrix decreased. The images further illustrate that the WC-12Co powder combinations were able to retain more carbide particles in comparison to the WC powder combinations.

From the XRD patterns of the powders and corresponding coatings depicted in Figs. 4 and 5, it is evident that no decarburization occurred during the cold CGDS of WC-xNi and WC-12Co-xNi. In addition, phase changes did not occur, implying that the chemical properties of the parent powders remain unchanged. No peak broadening as documented in the work conducted by Ang [19] was observed.

The adhesion characteristics of the coating were examined using elemental mappings of the interfaces. Since the journal is printed in black and white, the readers are advised to visit the internet version of this paper where the color is retained for a better study of the element distribution. Fig. 6 illustrates the mapping conducted on the WC-12Co-4Ni coating, which shows the distribution of the W [Fig. 6(a)], Co [Fig. 6(b)], Ni [Fig. 6(c)] and Fe [Fig. 6(d)]. The mapping clearly reveals that no atomic diffusion from the coating to the substrate took place at the interface during deposition. Minor traces of Fe were observed in the coating. This could be due to the powder contamination experienced during deposition. The hard carbide particles act as an

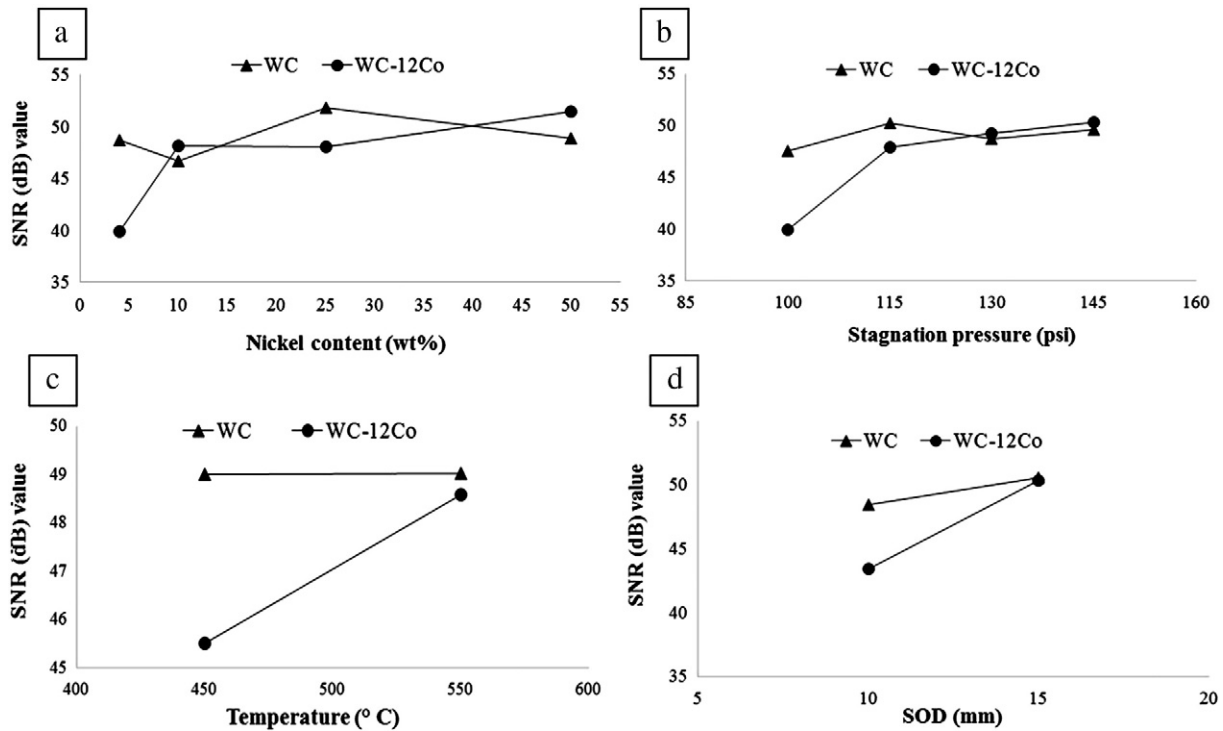


Fig. 2. Average SNR values for input process parameters studied.

abrasive, causing the Fe composed spray nozzle to wear rapidly and contaminate the powders as they pass through it.

A summary of the measured coating properties is listed in Table 4. It was observed that increasing the Ni content in the starting powders generally resulted in increased coating porosity and binder mean free path values. The exceptions to this trend were the higher porosity of the WC-25Ni compared to the WC-50Ni, and the higher porosity of the WC-12Co-4Ni compared to the WC-12Co-10Ni. Increasing the Ni content also led to a decrease in the percentage of WC retained which caused a subsequent decrease in the coating hardness. This is in agreement with Melendez and McDonald [22], who showed that increasing the carbide content in the starting powders resulted in an increase in the percentage of carbide retained in the resultant coating.

The WC-12Co-xNi powders yielded coatings that were more porous in comparison to the WC-xNi coatings even though lower stagnation pressures were required for the deposition of three of the four WC-xNi powders. The WC-12Co-xNi coatings had smaller binder mean free paths compared to the WC-xNi coatings for similar Ni contents. Overall, the 4 wt.% Ni addition for both powders yielded coatings with the highest hardness and percentage WC retained, and the lowest porosity and binder mean free paths. The WC-4Ni coatings possessed the maximum hardness of 459.2 HV<sub>0.3</sub> of all the eight powder combinations. This is still significantly lower than the hardness values typically observed for high pressure CGDS and HVOF produced WC-Co coatings, e.g. 1135 HV<sub>0.3</sub> for HVOF sprayed WC-12Co coatings [29]. The hardness values of the WC-25Ni coatings were comparable to those obtained by Melendez and McDonald [22]. Both the 50 wt.% Ni-WC and WC-12Co coatings possessed hardness values greater than those obtained by Melendez [22] using the same Ni content. The WC-12Co-xNi coatings

were also able to retain more carbide particles compared to the WC-Ni coatings. The highest carbide retention of 74.08% was achieved using the WC-12Co-4Ni composition.

Fig. 7 is a comparison of the hardness profiles of the WC-25Ni and WC-12Co-50Ni coatings. Hardness profiles could not be conducted on all eight coatings as some were too thin to allow for the required indent spacing as per ASTM C132 [27]. Overall, the WC-25Ni coatings had higher hardness values in comparison to the WC-12Co-50Ni coatings. As the distance from the interface increased, the hardness increased. At a distance of approximately 1000 μm from the interface, the hardness reached a maximum value and then decreased as the coating surface was approached. This behavior was observed for both coatings at similar positions.

#### 4. Discussion

In the current study the feasibility of using a Centerline SST low pressure CGDS system, with air as a carrier gas, to deposit WC-x wt.% Ni coatings onto mild steel was assessed. Gas temperature, stagnation pressure and standoff distance were varied in order to determine the optimal deposition parameters for each of the eight powder compositions according to the Taguchi method. Differences in the powder morphology will influence the optimal spray parameters and subsequently the coating properties obtained for each powder blend.

According to the work conducted by Phani et al. [30], it was found that the temperature of the inlet gas temperature was the most influential parameter on the coating properties followed by stagnation pressure and standoff distance, due to its drastic effect on particle velocity. Increasing the gas temperature has a minimal effect on the particle

Table 3

Comparison of experimental and theoretical response variables obtained using the Taguchi method.

Powder composition	Experimental		Theoretical	
	Thickness (μm)	Hardness (HV <sub>0.3</sub> )	Thickness (μm)	Hardness (HV <sub>0.3</sub> )
WC-25Ni	1828.13	403.6	583.41–772.21	283.13–338.09
WC-12Co-50Ni	560.43	210.6	759.27–949.68	293.62–360.50

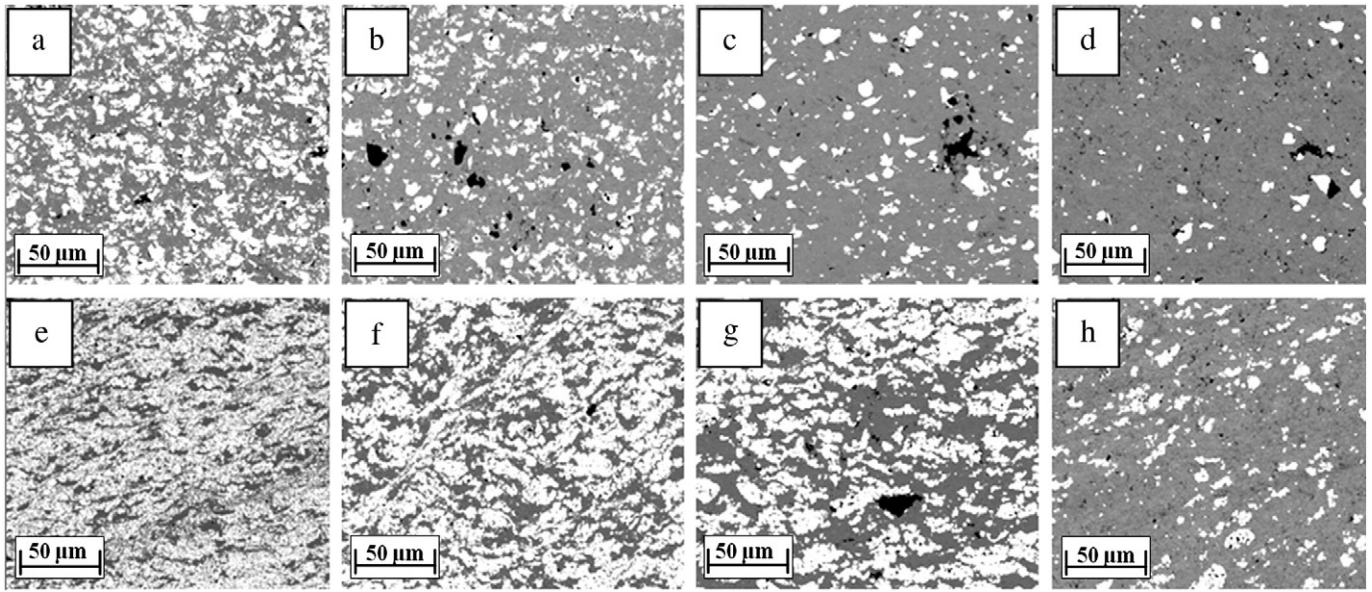


Fig. 3. Microstructure of all eight coatings with composition: (a)–(d) WC–xNi coatings and (e)–(h) WC–12Co–xNi coatings. White phase = WC, light gray phase = Co, dark gray phase = Ni matrix.

deposition temperature as the energy is expended on accelerating the particles to higher velocities. Upon heating, the gas rapidly expands in the divergent nozzle that results in higher particle velocities [23]. The stagnation pressure applied during deposition has a considerable influence on the coating hardness. At lower pressures, most of the particles are not deposited but are rebounded from the substrate. This results in a shot peening effect which improves particle bonding and increases the hardness of the coatings through work hardening as observed by Lee et al. [31]. The standoff distance used during deposition also plays

a significant role in the coating properties obtained, as it influences the gas velocity once the particles have emerged from the nozzle. SOD controls two competing mechanisms that affect particle velocity, namely, particle acceleration/deceleration due to the formed free gas jet and particle deceleration due to the presence of the bow shock that increases the drag force experienced by the particles [32]. In this study, Pattison et al. [32] demonstrated that the occurrence of bow shock reduced both the velocity of the carrier gas and the entrained particles. At low standoff distances, the effect of the bow shock was

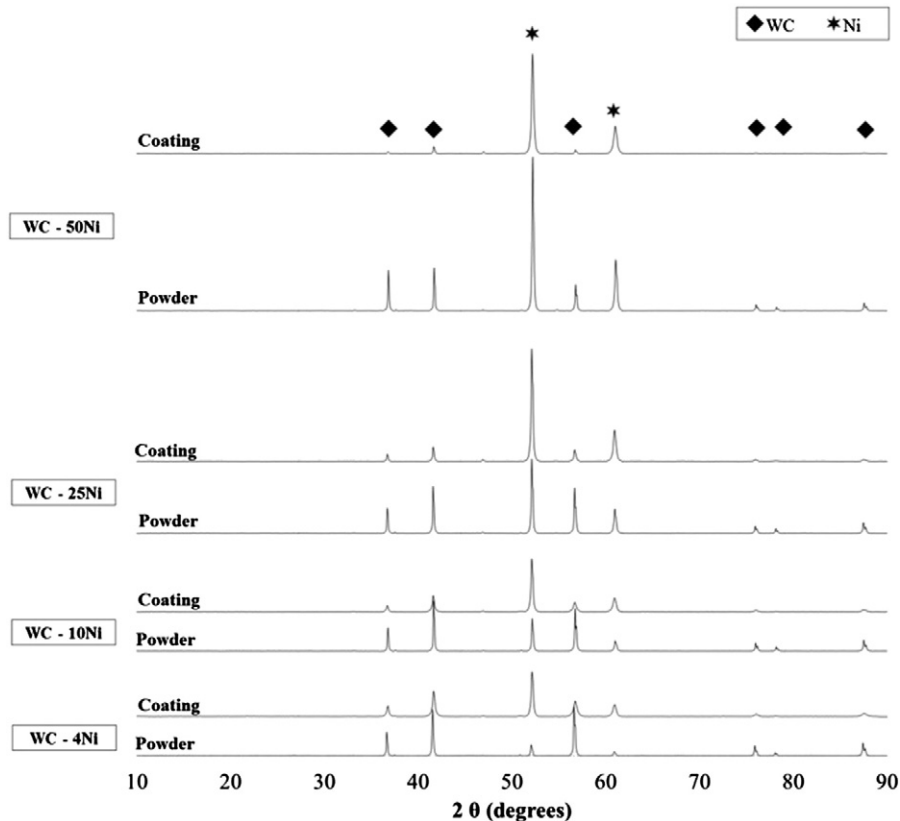


Fig. 4. XRD patterns of WC–x wt.% Ni powders and coatings.

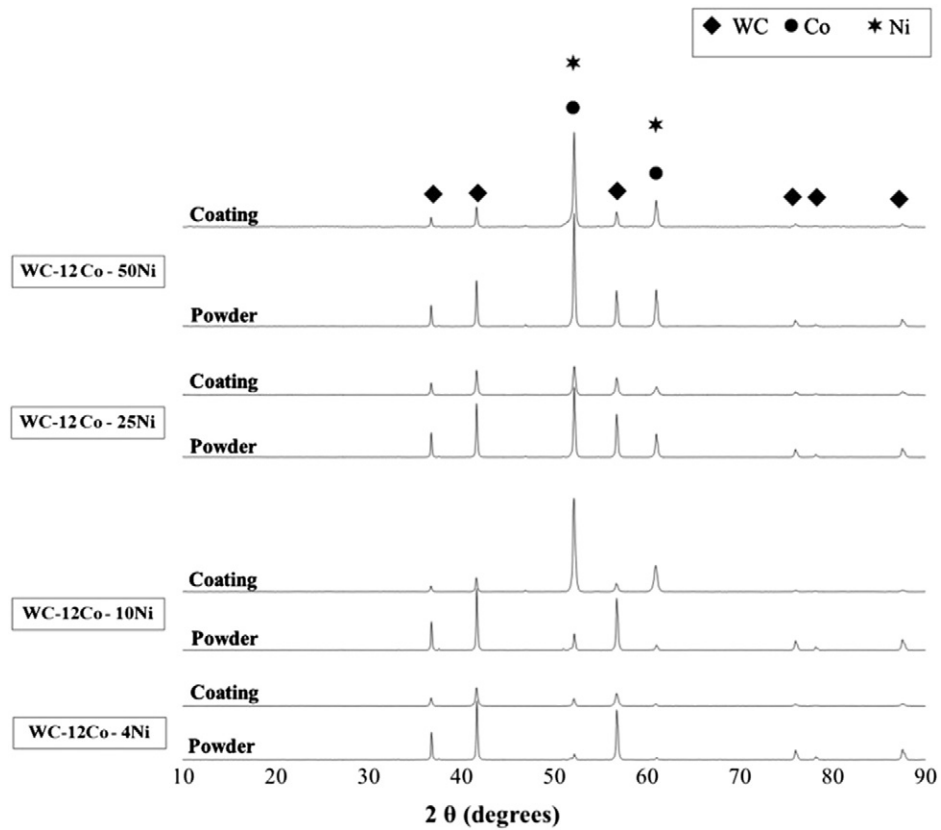


Fig. 5. XRD patterns of WC-12Co-x wt.% Ni powders and coatings.

pronounced resulting in decreased particle velocities and deposition efficiencies. At high standoff distances, the presence of the bow shock disappeared, however, the gas velocity had fallen below the particle velocity resulting in particles deceleration. For optimal deposition, it

was recommended that a region between the two distances be selected where the occurrence of bow shock has been eliminated.

As observed in Table 3, neither the coating thickness nor the hardness values obtained experimentally fell within the ranges predicted

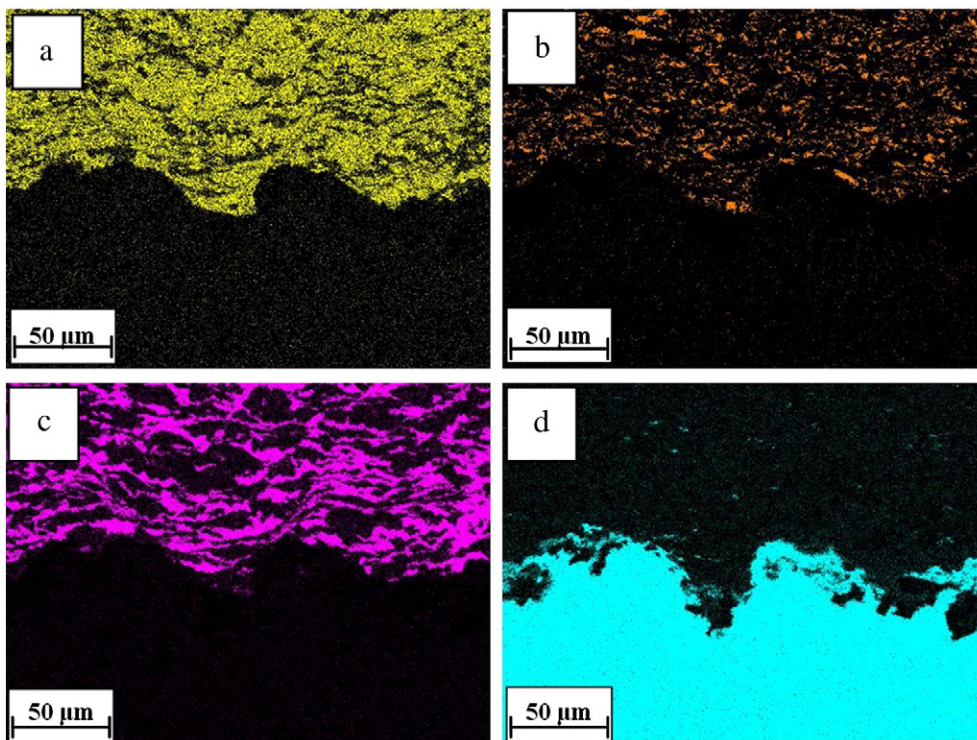


Fig. 6. Elemental composition maps of a WC-12Co-4Ni coating. (a) W. (b) Co, (c) Ni and (d) Fe.

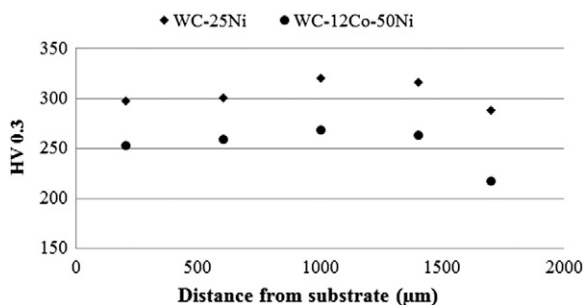
**Table 4**  
Coating properties.

Ni (wt.%)	Hardness (HV <sub>0.3</sub> )		Porosity (%)		Binder mean free path (μm)		% WC retained	
	WC	WC–12Co	WC	WC–12Co	WC	WC–12Co	WC	WC–12Co
4	459 ± 19	414.9 ± 23.2	1.47	3.51	5.42	1.77	39.89	74.08
10	391.5 ± 16.1	362.2 ± 32.6	2.27	3.15	12.54	3.10	24.47	63.54
25	305.6 ± 17.0	294.3 ± 31.6	2.70	3.79	21.21	4.85	17.07	47.92
50	275.8 ± 16.3	260.9 ± 25.4	2.49	5.11	48.59	10.09	6.92	27.06

by the Taguchi method. With CGDS, the deposition of hard and brittle materials such as carbides has proven unsuccessful unless co-deposited with a ductile metal in the form of a MMC. With the deposition of the WC–xNi and WC–12Co–xNi MMCs, the plastic material jet required for adhesion could only be formed for the Ni and not the WC particles, thus contributing to the failed Taguchi predictions. It was also proposed by Whitcomb and Anderson [33] that when applying the Taguchi technique, the factor levels selected for the experiments should be adjusted to bring the predicted values closer to the target, reducing the variability. One of the ways of achieving this is by selecting factor level values that are not too wide spread from one another. The Taguchi method is not good for dynamic systems. This was evident from the hardness profiles in Fig. 7 which showed that the coating hardness varies as a function of distance from the substrate–coating interface to the coating surface. The method does not take the occurrence of strain hardening, due to the impact of the hard carbide particles, into consideration and this causes deviations between the predicted and experimental values. The application of this technique is also limited in that it can only be applied at the initial stages of the process design system as to determine the parameter ranges that are most likely to yield optimal responses [34]. An iterative application of the method should therefore be applied until convergence between the predicted and experimental values is obtained, thereby improving the robustness of the technique.

Despite the limitations of the Taguchi method, the deposition of the two carbide powder blends, WC–xNi and WC–12Co–xNi, using low pressure CGDS was achieved even at Ni additions as low as 4 wt.%. As observed in the XRD patterns of both the WC–xNi and WC–12Co–xNi coatings presented in Figs. 4 and 5 respectively, the spray conditions applied did not cause decarburization, oxidation and phase changes typically observed in HVOF coatings [1,3,4,6–10]. As a result, the chemical composition and bulk properties of the coatings typically remain identical to the parent powders. Ang et al. [19] observed the occurrence of grain refinement in which higher deposition pressures, in the range of 174–218 psi, were used, and concluded that this was due to the severe plastic deformation experienced during particle impact. In the current work, the occurrence of possible grain refinement is still under study.

Three distinct phases were observed in the coatings as depicted in Fig. 3. The carbide particles were able to embed themselves in the softer Ni matrix during the deposition of WC–xNi and WC–12Co–xNi powders, proving that mechanically mixed powders can be used for low pressure CGDS. The microstructure revealed areas rich in Ni and carbide

**Fig. 7.** Hardness profiles of the WC–25Ni and WC–12Co–50Ni coatings.

(WC and WC–12Co) particles which led to the high standard deviation observed for the coating hardness values. The carbide content in the coatings was lower than that of the starting powders, in which the WC–12Co–xNi coatings had higher carbide retention properties in comparison to the WC–xNi coatings. The differences in the carbide content between the powders and coatings can be attributed to the occurrence of preferential deposition of the individual powder components which takes place during spraying. The ductile nature of Ni also makes it easier to deposit unlike the hard, brittle WC particles which shatter upon impact if deposited without a suitable binder.

Pure WC cannot be deposited without a binder using CGDS due to its hard and brittle nature. In the current study unsuccessful attempts were made to deposit agglomerated and sintered WC–12 wt.% Co powders using the low pressure CGDS system without the addition of mechanically mixed Ni powder. The process parameters for the low pressure CGDS are too low to allow for the adiabatic shear instability to take place and so allow for the material jet formation of the ductile Co binder component to occur. The Co binder is also embedded between the nano-sized WC grains, further decreasing its ability to deform and make contact with the substrate and neighboring particles during deposition. The addition of Ni to both the WC–12 wt.% Co and WC powders was therefore necessary to facilitate adhesion. The deposition of WC–Co powders has been achieved in previous studies by other authors, where high pressure CGDS systems were used [11–13,19,20], where pressures up to 300 psi were applied.

The deposition of all the powder combinations investigated, can therefore be attributed to the deformation and shearing of the ductile Ni binder during deposition. Lowering the binder content limits the coating build-up as seen with the 4 wt.% Ni blends. This relationship is summarized in Table 4. Lower Ni contents reduce powder ductility and the hard, brittle carbide phase acts as an erodent, chipping away the previously deposited layer. This further substantiates the occurrence of coating adhesion–erosion during the deposition of the MMC powders as observed by Schmidt et al. [23]. Increasing the Ni content led to increased coating thicknesses, however, compromising the hardness values. This is because the Ni binder is softer than the hard carbide phases. At higher stagnation pressures, the thickness of the WC–xNi coatings decreased, this is presumably due to the sharp angular nature of the micro-sized WC powder which also erodes the coating during deposition.

Changes in the morphology of the powders can be observed in both particle types (WC–xNi and WC–12Co–xNi) as a result of the deposition process. Fig. 8(a) reveals that the dense WC particle fracture as a result of the high impact energy experienced during deposition, however remained embedded within the Ni matrix. The fractured particles, coupled with the occurrence of porosity within the matrix decrease the coating hardness measured. In contrast, the spherical, agglomerated and sintered WC–12Co powder particles presented in Fig. 8(b) were flattened, elongating the particles across the nickel matrix. This particle behavior has also been observed during HVOF spraying and is attributed to the porous structure and deformability of the bimodal, spherical and agglomerated powders. Dosta [20] studied the effect of powder porosity on the deposition behavior of WC–25Co using CGDS. It was found that the porosity of the starting powder affected the deposition behavior of the particles and that porosity was essential for particle deformation. Fig. 9 illustrates the cross section of the WC and WC–12Co used in this

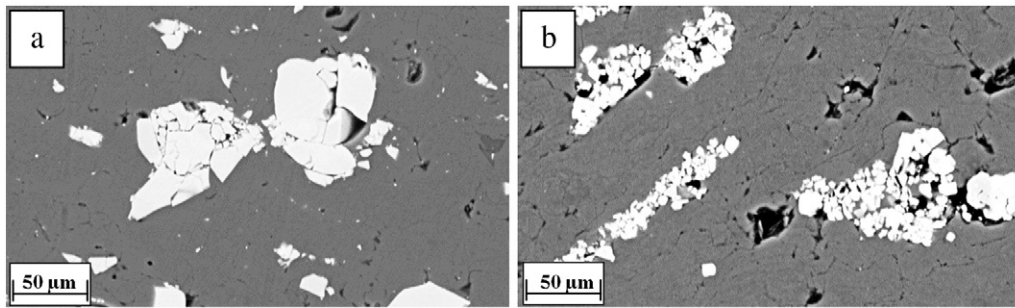


**Fig. 8.** SEM micrographs showing (a) fractured WC particles within Ni matrix, and (b) elongated and deformed WC–12Co agglomerates within Ni matrix as a result of the high energy impact experienced during deposition.

study, in which the porosity of the agglomerated and sintered WC–12Co powder was calculated to be 31%, classifying it as a high porosity powder. Similarly to the particles examined in the study by Dosta [20], the highly porous WC–12Co particles experienced much deformation and particle compaction during deposition as illustrated in Fig. 8(b). The porous nature of the spherical and agglomerated WC–12Co increased the deformability of the particles, allowing for particle densification and coating build-up. The deposition behavior of the oxide reduced WC particles resembled that of the low porosity WC–25Co agglomerated and sintered powders used in the study by Dosta [20] in that there was very little deformation of the particles during impact. However, the impact experienced was sufficient to shatter the WC particles during the deposition of the WC–xNi powders as observed in Fig. 8(a).

The distinct differences in particle morphology is a probable explanation for the higher carbide retention achieved with the WC–12Co based coatings in comparison to those formed by the WC powders. As previously discussed, lower percentages of retained carbide (WC and WC–12Co) particles were noted in the coatings compared to the amount present in the starting powders. This can also be attributed to the fact that the three starting powders, Ni, WC and WC–12Co, had different powder morphologies and densities. This influenced the resultant particle velocity within the moving carrier gas stream. The lighter, spherical and agglomerated nano-structured WC–12Co particles were able to achieve greater particle velocities during flight compared to the dense WC particles. However, the denser WC particles could have attained higher impact energies during impact, resulting in less porous coatings. It is hypothesized by the authors that higher carbide retention could have been attained by Melendez [22] had spherical and agglomerated WC–12Co powders been used instead of the angular, sintered and crushed powders used in their study. As discussed in literature, the high impact energies obtained by the WC powders pronounced coating erosion during deposition. In contrast, WC–12Co deposits better under higher pressures due to its porous and deformable nature.

Different levels of porosity were observed in all the coatings, with higher values found in the WC–12Co–xNi coatings, even though higher stagnation pressures were required for their deposition. This may be due to the highly porous nature of the WC–12Co agglomerate powder shown in Figs. 1(c) and 9(b). The WC–4Ni powder yielded coatings with the lowest porosity of 1.47% while the WC–12Co–50Ni coatings possessed the highest porosity of 5.11%. The pores present in the coatings decreased the hardness measured. The softer nature of the Ni binder also contributed to the low coating hardness values as it possesses hardness values which are substantially lower than carbide materials.

The hardness values obtained for the WC–12Co–4Ni coatings were slightly lower than those obtained by Melendez and McDonald [22]. It is postulated that Melendez [22] was able to achieve greater particle velocities by making use of an external volumetric powder feeder to introduce the powder particles into the moving gas stream. The increased particle velocity would have resulted in greater impact velocities, denser and harder coatings in comparison to when a non-pressurized vibratory powder feeder is used.

Material interlocking is also one of the key bonding mechanisms that occur during the cold gas deposition of powders onto a substrate. Elemental mapping of one WC–12Co coating depicted in Fig. 6 clearly reveals that no atomic diffusion took place at the interphase during deposition. This is an indication that material interlocking was obtained as the coatings were well adhered on the substrate.

## 5. Conclusions

Low pressure CGDS is suitable for the deposition of carbide particles, provided that a suitable ductile binder is selected to deposit the particles in the form of a cemented carbide. In the investigation conducted, cold spray Ni was able to successfully co-deposit both the WC and WC–12Co powders even at percentages as low as 4 wt.%. The binder content, together with the spray parameters had significant effects on the coating response variables measured. The Taguchi design of experiments

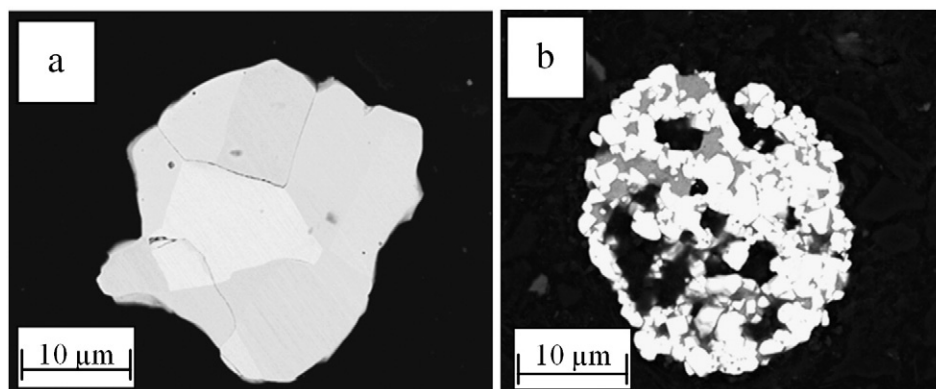


**Fig. 9.** Cross sections of (a) WC and (b) WC–12 wt.% Co powder particles.

tool used to determine the spray parameters of the powders was unable to successfully predict the coating hardness and thickness values to be obtained for the optimum WC–25Ni and WC–12Co–50Ni coatings. This is because the method does not account for the occurrence of strain hardening that takes place during deposition. XRD analysis of all eight coatings indicated that no phase transformations took place during deposition. Overall, dense coatings with some porosity and a non-homogenous distribution of the carbide phase were obtained for both the WC–xNi and WC–12Co–xNi combinations. In general, the WC–xNi coatings possessed higher hardness values in comparison to the WC–12Co–xNi coatings even though the latter coatings were able to achieve higher carbide retention. The WC–4Ni coatings possessed the maximum hardness of 459.2 HV<sub>0.3</sub> and lowest porosity of 1.47% out of all the eight powder combinations. Particle morphology greatly influenced the deposition behavior of both the WC and WC–12Co particles. The dense WC particles fractured as a result of the high energy impact process, however gave rise to less porous coatings with a higher hardness. The porous structure of the spherical and agglomerated WC–12Co powders was more deformable allowing for particle densification and elongation during deposition which resulted in higher carbide retention within the Ni matrix.

### Acknowledgments

The authors wish to acknowledge the financial support received from the Department of Science and Technology and the National Research Foundation in South Africa (grant no. 41292). Pilot Tools Pty, South Africa is acknowledged for the use of their facilities. The assistance of Mr. Agripa Hamweendo, Mr. Gerrard Peter and Mr. Shadrack Moqabulane is greatly appreciated.

### References

- [1] M. Watanabe, A. Owada, S. Kuroda, Y. Gotoh, Effect of WC size on interface fracture toughness of WC–Co HVOF sprayed coatings, *Surf Coat Technol* 201 (3–4) (2006) 619–627.
- [2] A. Zikin, S. Ilo, P. Kulu, I. Hussainova, C. Katsich, E. Badisch, Plasma transferred ARC (PTA) hardfacing of recycled hardmetal reinforced nickel-matrix surface composites, *Mater Sci* 18 (1) (2012) 12–17.
- [3] T. Sahraoui, T. Guessasma, M. Ali Jeridane, M. Hadji, HVOF sprayed WC–Co coatings: microstructure, mechanical properties and friction moment prediction, *Mater Des* 31 (3) (2010) 1431–1437.
- [4] Y. Qiao, T.E. Fischer, A. Dent, The effects of fuel chemistry and feedstock powder structure on the mechanical and tribological properties of HVOF thermal-sprayed WC–Co coatings with very fine structures, *Surf Coat Technol* 172 (1) (2003) 24–41.
- [5] P. Kulu, T. Pihl, Selection criteria for the wear resistant powder coatings under extreme erosive wear conditions, *J Therm Spray Technol* 11 (4) (2002) 517–522.
- [6] L. Jacobs, M.M. Hyland, M. De Bonte, Comparative study of WC–cermet coatings sprayed via HVOF and the HVAF process, *J Therm Spray Technol* 7 (2) (1998) 213–218.
- [7] B.H. Kear, R.K. Sadangi, M. Jain, R. Yao, Z. Kalman, G. Skandan, et al., Thermal sprayed nanostructured WC/Co hardcoatings, *J Therm Spray Technol* 9 (3) (2000) 399–406.
- [8] D.A. Stewart, P.H. Shipway, D.G. McCartney, Abrasive wear behaviour of conventional and nanocomposite HVOF-sprayed WC–Co coatings, *Wear* 225–229 (2) (1999) 789–798.
- [9] S. Usmania, S. Sampatha, D.L. Houckb, D. Leec, Effect of carbide grain size on the sliding and abrasive wear behavior of thermally sprayed WC–Co coatings, *Tribol Trans* 40 (3) (1997) 470–478.
- [10] D.A. Stewart, P.H. Shipway, D.G. McCartney, Microstructural evolution in thermally sprayed WC–Co coatings: comparison between nanocomposite and conventional starting powders, *Acta Mater* 48 (7) (2000) 1593–1604.
- [11] H. Kim, C. Lee, S. Hwang, Fabrication of WC–Co coatings by cold spray deposition, *Surf Coat Technol* 191 (2–3) (2005) 335–340.
- [12] H. Kim, C. Lee, S. Hwang, Superhard nano WC–12%Co coating by cold spray deposition, *Mater Sci Eng A* 391 (1–2) (2005) 243–248.
- [13] R.S. Lima, J. Karthikeyan, C.M. Kay, J. Lindemann, C.C. Berndt, Microstructural characteristics of cold-sprayed nanostructured WC–Co coatings, *Thin Solid Films* 416 (1–2) (2002) 129–135.
- [14] A. Papyrin, V. Kosarev, S. Klinkov, A. Alkhimov, V. Fomin, *Cold Spray Technology*, 1st ed. Elsevier, 2006.
- [15] S. Kuroda, J. Kawakita, M. Watanabe, H. Katanoda, Warm spraying – a novel coating process based on high-velocity impact of solid particles, *Sci Technol Adv Mater* 9 (3) (2008) 1–17.
- [16] T. Hussain, D.G. McCartney, P.H. Shipway, D. Zhang, Bonding mechanisms in cold spraying: the contribution of metallurgical and mechanical components, *J Therm Spray Technol* 18 (3) (2009) 364–379.
- [17] J. Villafuerte, Current trends in cold spray technology: looking at the future, *Met Finish* 108 (1) (2010) 37–39.
- [18] X. Ning, J. Jang, H. Kim, The effects of powder properties on in-flight particle velocity and deposition process during low pressure cold spray process, *Appl Surf Sci* 253 (18) (2007) 7449–7455.
- [19] A. Ang, C. Berndt, P. Cheang, Deposition effects of WC particle size on cold sprayed WC–Co coatings, *Surf Coat Technol* 205 (10) (2011) 3260–3267.
- [20] S. Dosta, M. Couto, J.M. Guilemany, Cold spray deposition of a WC–25Co cermet onto Al7075-T6 and carbon steel substrates, *Acta Mater* 61 (2) (2013) 643–652.
- [21] J. Wang, J. Villafuerte, Low pressure cold spraying of tungsten carbide composite coatings, *Adv Mater Process* 167 (2) (2009) 54–56.
- [22] A. Melendez, A. McDonald, Development of WC-based metal matrix composite coatings using low-pressure cold gas dynamic spraying, *Surf Coat Technol* 214 (2013) 101–109.
- [23] T. Schmidt, F. Gärtner, H. Assadi, H. Kreye, Development of a generalized parameter window for cold spray deposition, *Acta Mater* 54 (2006) 729–742.
- [24] T. Goyal, R.S. Walia, T.S. Sidhu, Multi-response optimization of low-pressure cold-sprayed coatings through Taguchi method and utility concept, *Int J Adv Manuf Technol* 64 (2013) 903–914.
- [25] T. Goyal, R.S. Walia, T.S. Sidhu, Effect of parameters on coating density for cold spray process, *Mater Manuf Process* 27 (2) (2012) 193–200.
- [26] T. Goyal, R.S. Walia, T.S. Sidhu, Study of cold spray process for coating thickness using Taguchi method, *J Mater Manuf Process* 27 (2) (2012) 185–192.
- [27] ASTM Standard E384-11e1, Standard Test Method for Knoop and Vickers Hardness of Materials, ASTM International, West Conshohocken, 2011. [www.astm.org].
- [28] C. Smith, L. Guttman, Measurement of internal boundaries in three dimensional structures by random sectioning, *AIME Trans* 197 (1953) 81–87.
- [29] J. He, M. Ice, S. Dallek, E.J. Lavernia, Synthesis of nanostructured WC–12 Pct Co coating using mechanical milling and high velocity oxygen fuel thermal spraying, *Metall Mater Trans* 31A (2005) 541–553.
- [30] P.S. Phani, D.S. Rao, S.V. Joshi, G. Sundararajan, Effect of process parameters and heat treatments on properties of cold sprayed copper coatings, *J Therm Spray Technol* 16 (3) (2007) 425–434.
- [31] H. Lee, H. Shin, S. Lee, K. Ko, Effect of gas pressure on Al coatings by cold gas dynamic spray, *Mater Lett* 62 (2008) 1579–1581.
- [32] J. Pattison, S. Celotto, A. Khan, W. O'Neill, Standoff distance and bow shock phenomena in the cold spray process, *Surf Coat Technol* 202 (2008) 1443–1454.
- [33] P.J. Whitcomb, M.J. Anderson, Robust design – reducing transmitted variation: finding the plateaus via response surface methods, *ASQC Qual Cong Proc* 50 (1996) 642–651.
- [34] Unitek Miyachi Group, Welding material control, *Tech Appl Brief* 2 (1999) 1–5.